Brightness measurements of a gallium liquid metal ion source

C. W. Hagen,[a] E. Fokkema, and P. Kruit
Faculty of Applied Sciences, Delft University of Technology, Lorentzweg 1, 2628CJ Delft, The Netherlands

(Received 17 June 2008; accepted 25 August 2008; published 1 December 2008)

The virtual source size of a liquid metal ion source is an order of magnitude larger than the size of the region from which the ions are emitted at the source. This source size has a direct effect on the reduced brightness and, hence, on the performance of these sources. The variation of the virtual source size of a gallium liquid metal ion source as a function of the angular current density at the source has been measured. This was done by measuring the source image size from images of a pencil lead sample taken with an FEI focused ion beam system. The measurements indicate that the virtual source size grows from about 50–80 nm when the emission current increases from 1 to 10 μA. The experimental data on the virtual source size are compared with the theory on stochastic Coulomb interactions in the source region. On the basis of these measurements the authors show that the reduced brightness deteriorates with an increasing angular current density. The maximum reduced brightness measured was 1×10^6 A/(m^2 sr V). © *2008 American Vacuum Society.* [DOI: 10.1116/1.2987958]

I. INTRODUCTION

The gallium liquid metal ion source (LMIS) is the most commonly used source in focused ion beam (FIB) systems.[1] It consists of a tungsten wire etched into a blunt tip. The tip is covered with liquid gallium which, in an applied electrostatic field, takes the shape of a cone (the so-called Taylor cone) elongated into a cusp with a spherical tip.[2] Positive ions are emitted from the apex of that tip when the applied field is larger than a certain threshold value. The ion current then rises sharply to a value of typically 1 μA, the onset current, followed by a linear increase with the applied field. Simulations and measurements have shown that, for currents smaller than ~10 μA, the length of the cusp is almost zero but increases significantly at higher emission currents.[2] The radius of the cusp is estimated from transmission electron micrographs as 1.5 nm,[3] a value that was recently found to be in agreement both with the electrohydrodynamics of the source[4] and with simulations of the source energy spread.[5] One would expect the virtual source size of the LMIS, i.e., the apparent source size looking back through an optical system, to be of the order of the cusp radius, i.e., 1.5 nm. However, the experimentally observed virtual source size is about 50 nm. For instance Komuro *et al.*[6] estimated the virtual crossover diameter of the source to be 40–45 nm from line-etching experiments on silicon and gallium arsenide substrates.

This has an important effect on the reduced brightness, which is often defined as

$$B_r = \frac{J_\Omega}{\frac{\pi}{4} d_s^2 U}, \tag{1}$$

with U the beam potential, d_s the diameter of the virtual source size, and J_Ω the angular current density. The reduced brightness is a conserved quantity in particle optics systems and determines the current I_i in an image of the source as

$$I_i = \frac{\pi^2}{4} \cdot B_r \cdot d_i^2 \cdot \alpha_i^2 \cdot U, \tag{2}$$

where d_i is the source image diameter and α_i is the beam half-opening angle in the image plane. With a virtual source size of 50 nm instead of 1.5 nm the reduced brightness is roughly three orders of magnitude smaller than expected and consequently a thousand times less current can be obtained in a focused image of the source.

The large virtual source size may be caused by reasons such as electrohydrodynamic instabilities, mechanical instabilities (vibrations), or aberrations of the accelerating field, but many authors have suggested a role for stochastic interactions between the ions. This is where we shall concentrate our efforts.

First Ward and Seliger[7] did trajectory calculations in the extraction region of a LMIS based on a continuous space-charge distribution. They showed that space charge increases the beam divergence near the emitter tip. Then Knauer[8] was one of the first to conclude that stochastic Coulomb interactions are responsible for the virtual source enlargement. Knauer's potential energy conversion theory led to a two-third power dependency on the current density. Later on Ward[9] did a Monte Carlo calculation of the virtual source size of a LMIS and concluded that the virtual source size enhancement is the result of random trajectory displacements caused by the random fluctuations in the transverse electric field. His calculations were, however, done for a single current, and he predicted a virtual source size of 50–100 nm.

Bi *et al.*[10] measured the probe size of a Ga^+-LMIS FIB system in different operation modes by scanning the beam over a knife edge. They found that Coulomb effects in the column deteriorate the probe size even at a probe current lower than 100 pA. At first they assumed that the current density distribution of the measured probe is Gaussian but

[a]Electronic mail: c.w.hagen@tudelft.nl

later Bi *et al.*[11] investigated the role of the Coulomb interactions on the tails of the current density distribution and showed that the tails are enhanced by the Coulomb interactions. All their work was concerned with interactions in the beam, not in the gun area and they started with the assumption of a 50 nm virtual source size.

Very recently Radlička and Lencová[5] published computation results on the virtual source size and energy spread based on a direct numerical integration of the equation of motion in a numerically calculated field for various tip dimensions. They included the stochastic interactions between the particles and were able to show that these can fully account for the 50 nm large virtual source size, assuming a source tip radius of 1.86 nm.

So far no experimental results of the enlargement of the virtual source size as a function of source operating conditions have been published. All above mentioned papers indicate that it is interesting to see how the source image size, and thus the virtual source size, changes with the emission current. It is the objective of this work to experimentally investigate the virtual source size as a function of the source operating conditions.

II. COULOMB INTERACTIONS

The interactions between charged particles based on the repulsive Coulomb force can be described as the combination of an average space charge and individual statistical interactions.[12,13] The space charge effect causes a deflection of the ions from the center of the beam and thus a defocus and aberrations. In this work we will not consider this effect because the defocus is easily removed by refocusing of the lenses and if the aberrations would contribute, the virtual source size would depend on the acceptance angle. This seems not to be the case, judging from some experiments we did with larger acceptance angles.

The transverse components of the statistical interactions cause random trajectory displacements. Interactions between particles are referred to as collisions and they have been modeled by Jansen.[13] These effects become dominant in narrow beams of low and moderate density. FIB instruments are especially sensitive to these interactions, because the particle density is higher and the time of flight through the system is longer than that of the faster moving electrons in an electron beam. Typical beam parameters for an ion beam where these interactions become important are 30 kV acceleration from a LMIS at currents above 0.1 nA.[12] It is important to discriminate between the interaction in the gun region and the interactions after the beam defining aperture in the column, especially at lower currents. In the gun region, where the number of ions is much larger, the ions are typically very close to each other and there is much more interaction than in the column.

The trajectory displacement effect can modify the trajectories of the particles traveling in a beam, resulting in a larger source image size. The basis for this effect is that a collision between particles can change the direction of a particle by $\Delta\alpha$. How much the particle deviates from its primary trajectory depends on the distance to the point of collision $z_{\text{collision}}$. If the angular displacement $\Delta\alpha$ is known, the spatial displacement Δr for small angles at a certain position z is given by

$$\Delta r = \Delta\alpha \cdot |z - z_{\text{collision}}| = \Delta\alpha \cdot \Delta z. \tag{3}$$

If Δr is directed away from the beam axis the trajectories of the particles move away from this axis and the beam broadens. If there is only one collision per particle the spatial displacement is calculated with Eq. (3), if one can model the distribution of distances between particles. This leads to closed expressions for the blur distribution in cylindrical beam segments, or segments with a crossover as given by Jansen's theory.[13] The expressions for the trajectory displacement effect are given for three different regimes. Now we will shortly describe these regimes. The first regime is known as the pencil beam regime. In this regime the average axial distance between the particles is much larger than the beam radius. In this case the average axial distance and not the beam geometry determines the strengths of the repulsive forces. The second regime is known as the Holtzmark regime, where the lateral dimension of the beam plays a role as it is large relative to the separation of the particles. Finally a high particle density leads to the Gaussian regime, where the particles have multiple collisions.

In the Holtzmark regime the angular displacement, and thus the trajectory displacement effect, is proportional to the two-third power of the angular current density, i.e.,[12]

$$\Delta\alpha \sim J_{\Omega}^{2/3}. \tag{4}$$

This is valid in a beam segment with a crossover as well as in a homocentric cylindrical beam.[13] If the form of the segments is complicated, with acceleration or deceleration or lens effects, it is impossible to derive a closed expression for the trajectory displacement effect. However, Eq. (4) still remains valid in the Holtzmark regime.

To obtain a rough estimate of the effect of the trajectory displacements in the source area we can calculate the FW50 in the Holtzmark regime for a conical beam segment of length L at a constant beam voltage U from[12]

$$\text{FW50} = 0.367 \frac{m^{1/3}}{\varepsilon_0} \frac{J_{\Omega}^{2/3} L^{2/3}}{U^{4/3}}, \tag{5}$$

with m the mass of the mass of a gallium ion (1.21×10^{-25} kg) and ε_0 the dielectric constant. Assuming an angular current density of 20 μA/sr, a length of the source region $L=30$ mm and $U=30$ kV, the FW50 of the trajectory displacements becomes about 16 nm. This is in fact an underestimation of the FW50 because in reality the ions are not at constant potential but are accelerated from 0 to 30 kV. It is interesting that Eq. (5) already predicts a value for the trajectory displacements of the right order of magnitude.

III. EXPERIMENTAL SETUP AND METHOD

Experiments were done in an FEI Strata 235 dual beam system. A schematic drawing of the ion beam column of that instrument is depicted in Fig. 1. The tip potential is at 30 kV

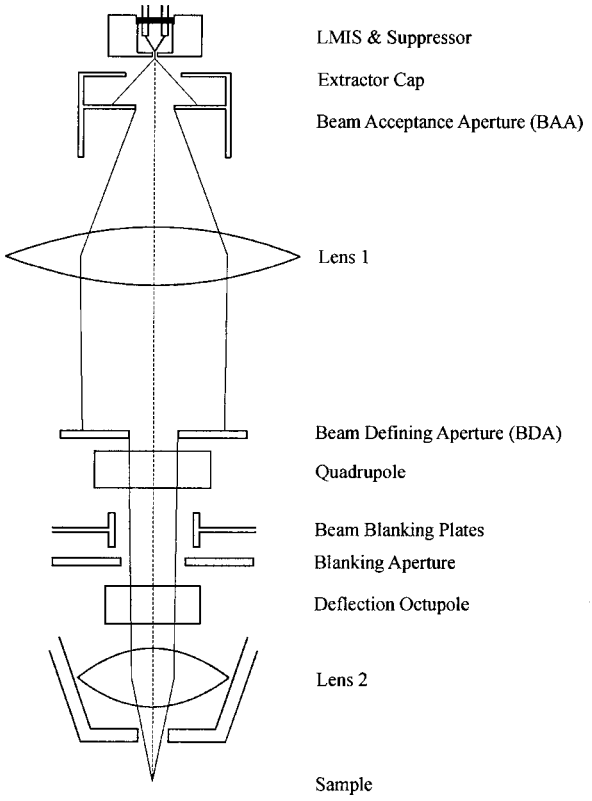

FIG. 1. Schematic outline of the FEI ion optical column. The ions extracted from the LMIS are focused with two three-electrode electrostatic lenses onto the sample. Note that the drawing is not to scale.

and the extractor is fixed at 12 kV below the tip potential. The first lens is a three-electrode accelerating lens. The beam defining aperture (BDA) which limits the current in the system is at ground potential. Ions emitted from the tip are thus accelerated to a 30 keV beam energy. After the ions are accelerated they are stigmated and focused onto a sample with a three-electrode electrostatic objective lens. The sample imaging is done with the ion induced secondary electrons which are detected by a channeltron detector.

The method we use to determine the virtual source size d_s is an indirect method. First we will measure the probe size d_p. The probe size contains several contributions: the source image contribution, the chromatic aberration contribution, the spherical aberration contribution, and the diffraction contribution. The latter can safely be neglected in FIB systems, because of the small wavelength of the ions. Of the aberration contributions usually the dominant one is the chromatic aberration contribution. Therefore we neglect the spherical aberration contribution here. The source image size d_i is the magnified image of the virtual source size d_s given by

$$d_i = M \cdot d_s, \tag{6}$$

where M is the column magnification of the two-lens system. The chromatic aberration contribution to the spot size, d_c, is given by[14]

$$d_c = 0.6 C_c \frac{\Delta E_{\mathrm{FW50}}}{E} \alpha_i, \tag{7}$$

where C_c is the coefficient of chromatic aberration, ΔE_{FW50} is the smallest width of the energy distribution containing 50% of the current, E is the beam energy, and α_i is the half-opening angle of the beam at the probe. This contribution may play an important role since the energy spread is about 5 eV.[2] The total diameter of the probe is given by

$$d_p^2 = d_i^2 + d_c^2. \tag{8}$$

When we limit α_i to small values only, the chromatic aberration contribution to the probe can be neglected. This is achieved by choosing the beam defining aperture sufficiently small. In our setup we chose an aperture of 20 μm diameter (the "10 pA aperture"). From simulations of the optical column it was verified that with this aperture the contribution of the chromatic aberration to the probe is much smaller than that of the source image. In that case the probe size is equal to the source image size, or $d_p = d_i$. So if we measure the probe size, the virtual source size d_s is easily determined by dividing d_p by the column magnification M, as it directly follows from Eq. (6). M is obtained from a simulation of the optical system.

It is noted here that there are different probe size measures. Often, full width at half maximum values are used, i.e., the width of the current distribution in the probe at half height. This is not a good measure for probe sizes, especially if the distribution has long tails as is the case in FIB systems. A good measure for probe sizes is the FW50, i.e., the full width of the probe area that contains 50% of the current. This measure can also be used to calculate the brightness, using Eq. (1) or (2). All diameters in this paper are FW50 values, unless stated otherwise.

From images of a sample containing many sharp edges we determine the probe size. This is done using an algorithm that finds all significant edges, i.e., light-dark transitions, in the image. For each edge it determines the 25%–75% width, i.e., the width between 25% and 75% of the intensity difference across the edge. The average width of all edges, after discarding extreme values, we take as the d_{25-75} probe size.[15] This size can conveniently be converted to the FW50 probe size without having to know the shape of the probe,[16]

$$d_{\mathrm{FW50}} = 1.76 d_{25-75}. \tag{9}$$

IV. RESULTS

The specimen we used to take the images is pencil lead (graphite), because it contains many sharp edges and it is quite resistant against milling. Figure 2 shows an image of the specimen made with the ion beam.

The probe size has been determined for various emission currents ranging from 1 to 10 μA, by applying different potentials to the suppressor. To verify the two-third-power dependence on the angular current density in the gun area $J_{\Omega,s}$, the angular current density has to be determined. $J_{\Omega,s}$ can be

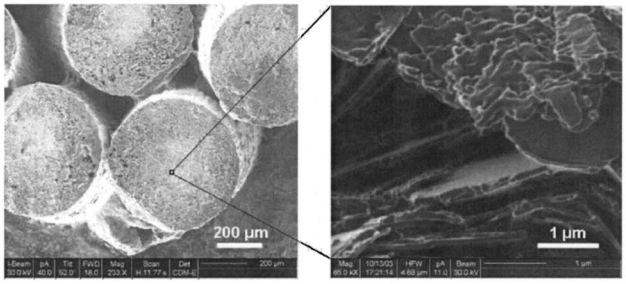

FIG. 2. SEM images of the pencil lead specimen.

calculated from the current behind the beam defining aperture, i.e., the probe current I_i, and the half-opening angle at the source α_s through

$$J_{\Omega,s} = \frac{I_i}{\pi \alpha_s^2}. \tag{10}$$

And α_s can be calculated from the half-opening angle at the probe α_i as

$$\alpha_s = \frac{\alpha_i}{M_a}, \tag{11}$$

where M_a is the total angular magnification of the two lens system. The half-opening angle at the probe α_i is easily obtained from the geometry of the system. Figure 3 shows part of the geometry: the objective lens and the beam defining aperture. For example, for a diverging incident ray, as sketched in Fig. 3, we obtain, using the magnification M_{obj} of the objective lens,

$$\alpha_i = \frac{\alpha_0}{M_{\text{obj}}} = \frac{r_\alpha}{v - l}\frac{1}{M_{\text{obj}}} = \frac{r_a}{b - M_{\text{obj}} l}, \tag{12}$$

in which v is the object distance, b the image distance, l is the distance between the BDA and the objective lens, α_0 the half-opening angle at the object side of the lens, and r_a is the radius of the BDA. The distances are known for the ion column and the magnifications were obtained from simulations using the Electrostatic Lens Design package by soft-

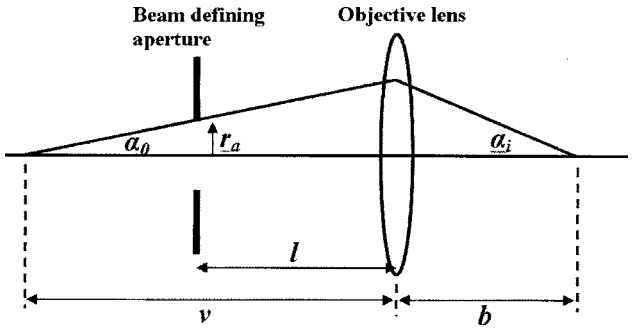

FIG. 3. Schematic drawing to illustrate how the half-opening angle at the probe α_i is calculated from the geometry of the optical system (v is the object distance, b the image distance, l is the distance between the BDA and the objective lens, α_0 the half-opening angle at the object side of the lens, and r_a is the radius of the BDA). Note that the angles are largely exaggerated for illustration purposes. In reality they are much smaller.

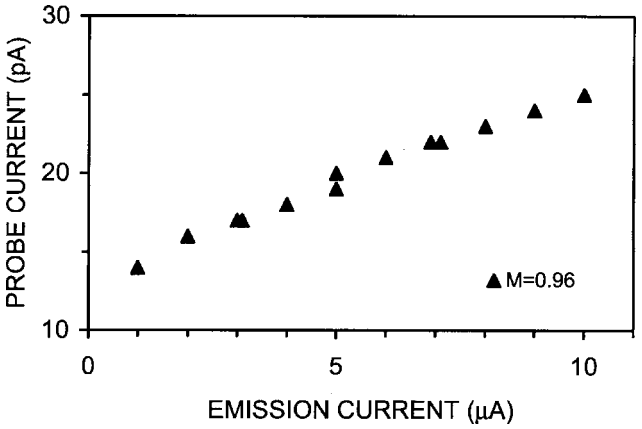

FIG. 4. Probe current as a function of the emission current in a FIB column with a beam defining aperture of 10 μm radius.

ware for particle optics computations (SPOC).[17] The lens settings used were 18 kV, −26950 V, and 0 V on the first, middle, and third electrodes of the first lens respectively, and 0, 17256, and 0 V on the first, middle, and third electrode of the objective lens respectively, resulting in a total magnification of 0.96.

When changing the emission current from 1 to 10 μA the corresponding beam current behind the beam defining aperture increases from 14 to 25 pA. The beam currents were measured using a Faraday cup. An emission current lower than about 0.7 μA would cause the source to become unstable and finally stop emitting. Figure 4 shows the measured probe current as a function of the emission current. The fact that the probe current does not increase by the same factor as the emission current means that the emission angle is increasing with emission current as well. This is due to the space charge in front of the source.[18] Although this space charge lens adds to the total magnification, especially at higher emission currents, its contribution is not precisely known. Therefore we chose to convert the probe current into the source angular current density using Eqs. (10)–(12) and in Fig. 5 the result is plotted versus emission current. The measured probe diameters d_{25-75} are plotted versus emission current in Fig. 6, and Fig. 7 shows the FW50 values of the

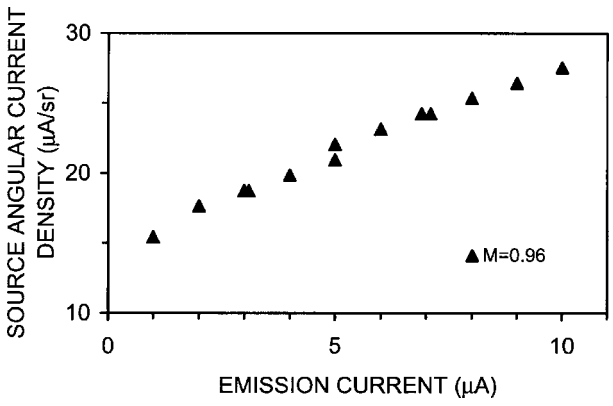

FIG. 5. Angular current density at the source vs ion emission current.

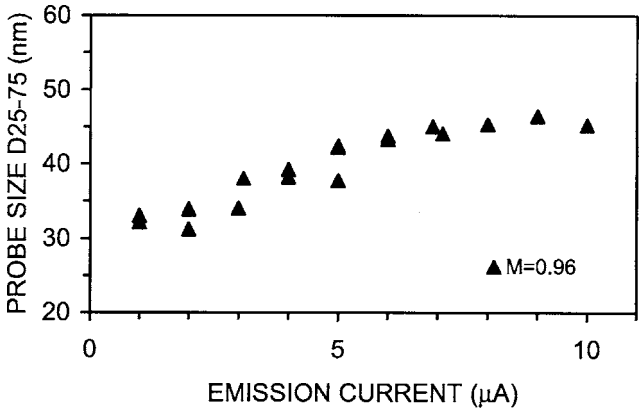

FIG. 6. Measured d_{25-75} probe sizes as a function of the ion emission current.

probe size as a function of the source angular current density. As the calculated total magnification is 0.96 this figure in fact shows the increase of the virtual source size with source angular current density, increasing from 50 to almost 80 nm for an angular current density increase from 15 to 30 μA/sr. We note that the contribution to the magnification of the space charge close to the emitter is neglected here. Figure 8 shows the same data as Fig. 7 but on a log-log scale. The data agree well with the 2/3-power law valid in the Holtzmark regime which is plotted in Fig. 8 as well (the drawn line).

Using Eqs. (2) and (12) and the measured probe sizes and probe currents, we can calculate the reduced brightness as a function of source angular current density. The result is shown in Fig. 9, revealing a decreasing reduced brightness with increasing angular current density. Similar experiments done in another Strata Dual Beam system, to demonstrate the reproducibility, led to very similar results and are therefore not shown here.

V. DISCUSSION

Without the influence of aberrations and because the experiments were done with a column magnification of ~1, the FW50 probe sizes shown in Figs. 7 and 8 are a good estimate of the virtual source size. The virtual source size at low

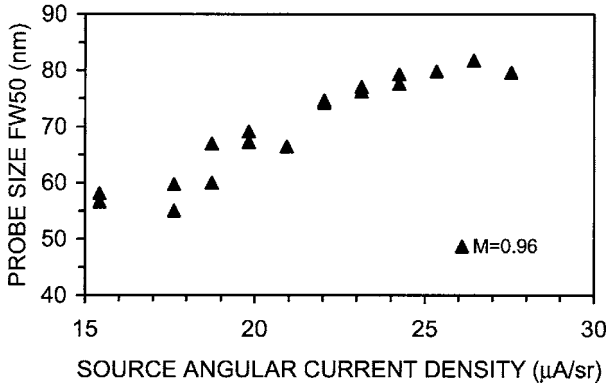

FIG. 7. FW50 probe sizes vs source angular current density.

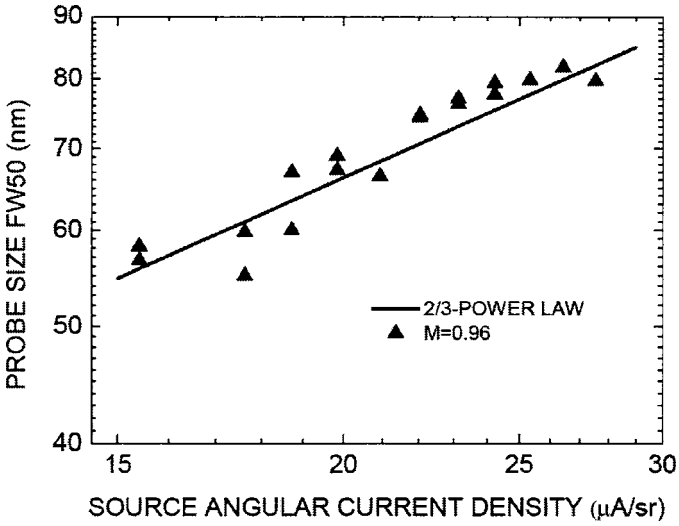

FIG. 8. Log-log plot of the FW50 probe sizes vs source angular current density. The solid line is the 2/3-power law describing the trajectory displacements due to the stochastic Coulomb interactions in the Holtzmark regime.

angular current density agrees well with measurements and Monte Carlo simulations of others.[5,6,9] The increase of the virtual source size at higher angular current densities scales well with the 2/3-power law, and therefore indicates that the large virtual source sizes are caused by the Coulomb interactions in the Holtzmark regime indeed.

Since we used a 10 pA aperture the current in the beam was very small compared to that in the gun region. From other studies we know that the pencil beam regime is valid in the column after such a small beam defining aperture.[12] In this case it is evident that Coulomb interactions in the column in the pencil beam regime do not contribute to the virtual source size at all. However, when a larger aperture is used the column might well be in the Holtzmark regime and the trajectory displacement effect will become significant there.

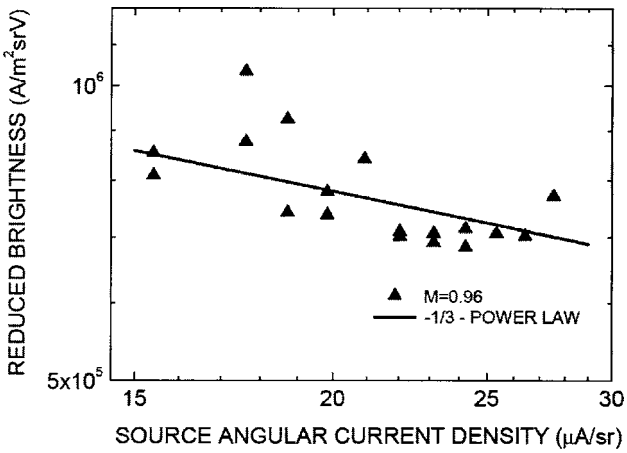

FIG. 9. Experimentally determined reduced brightness is seen to decrease as a function of the source angular current density. The solid line is the theoretical −1/3-power law describing the trajectory displacements due to the stochastic Coulomb interactions in the Holtzmark regime.

Our results show that the growth of the virtual source size due to Coulomb interactions causes the reduced brightness to deteriorate. This directly limits the resolution of the optical system. The reduced brightness B_r is inversely proportional to the square of the virtual source size diameter d_s and now that we know that $d_s \sim J_{\Omega,s}^{2/3}$, the reduced brightness can be written as

$$B_r \sim \frac{J_{\Omega,s}}{d_s^2} \sim J_{\Omega,s}^{-1/3}. \tag{13}$$

Equation (13) is drawn in Fig. 9 as a line with a slope of $-1/3$. The reduced brightness value at low angular current density of about 10^6 A m^{-2} sr^{-1} V^{-1} is in good agreement with measured values from literature.[19,20]

The deteriorating brightness at higher angular current densities has consequences for realistic probes. Inserting Eqs. (2) and (7) in Eq. (8) we obtain

$$d_p^2 = d_i^2 + d_c^2 \sim \frac{1}{B_r \alpha_i^2} + \Delta E_{\mathrm{FW50}}^2 \alpha_i^2. \tag{14}$$

From this equation it is seen that there is obviously an optimum α_i which minimizes d_p.

Inserting the optimum values in Eq. (2) the optimum current I_{opt} in a spot with diameter d is

$$I_{\mathrm{opt}} = 1.7 \frac{d^4 B_r E^3}{C_c^2 \Delta E_{\mathrm{FW50}}^2}. \tag{15}$$

This holds for an optimized instrument in a chromatic aberration limited situation. ΔE_{FW50} is known to increase with emission current[21] and therefore will also increase with angular current density. According to Jansen's theory[13] $\Delta E_{\mathrm{FW50}} \sim J_{\Omega,s}^{2/3}$ in the Holtzmark regime. So for the optimum current I_{opt} in a given spotsize we now find

$$I_{\mathrm{opt}} \sim J_{\Omega,s}^{-5/3}. \tag{16}$$

From Eq. (16) we see that it pays off to work at the lowest possible angular current density, if we want a substantial current in a small probe. However, this is limited by the intrinsic hydrodynamics.[2] The minimum stable emission current for a gallium LMIS is around 0.7 μA. as we have seen in our own experiments as well.

VI. CONCLUSIONS

We determined the virtual source size as a function of the emission current and thus as a function of angular current density by measuring the source image size. A virtual source size increase from 50 to 80 nm was found for an emission current increasing from 1 to 10 μA. The corresponding currents in the probe varied from 14 to 25 pA. The virtual source size dependence on angular current density in these experiments is in reasonable agreement with the theory of stochastic Coulomb interactions in the Holtzmark regime. Furthermore we showed that the reduced brightness deteriorates with an increasing angular current density.

ACKNOWLEDGMENTS

The authors gratefully acknowledge the following persons who contributed in some way to the results presented: M. Lysaght, S. Kellogg, G. A. Schwind, M. Straw, and P. Tesch at FEI Company, Hillsboro; P.F.A. Alkemade from the Kavli Institute, A.D. van Langeveld and J.E. Barth from the Department of Imaging Science and Technology, all at the Delft University of Technology.

[1] G. L. R. Mair, in *Handbook of Charged Particle Optics*, edited by J. Orloff (CRC, Boca Raton, FL, 1997), p. 103.
[2] R. G. Forbes, Vacuum **48**, 85 (1997).
[3] G. Benassayag, P. Sudraud, and B. Jouffrey, Ultramicroscopy **16**, 1 (1985).
[4] R. G. Forbes, Ultramicroscopy **108**, 455 (2008).
[5] T. Radlička and B. Lencová, Ultramicroscopy **108**, 445 (2009).
[6] M. Komuro, T. Kanayama, H. Hiroshima, and H. Tanoue, Appl. Phys. Lett. **42**, 908 (1983).
[7] J. W. Ward and R. L. Seliger, J. Vac. Sci. Technol. **19**, 1082 (1981).
[8] W. Knauer, Optik (Stuttgart) **59**, 335 (1981).
[9] J. W. Ward, J. Vac. Sci. Technol. B **3**, 207 (1985).
[10] J. Bi, X. R. Jiang, and P. Kruit, Microelectron. Eng. **35**, 439 (1997).
[11] J. Bi, P. W. H. de Jager, J. E. Barth, and P. Kruit, Microelectron. Eng. **41/42**, 249 (1998).
[12] P. Kruit and G. H. Jansen, in *Handbook of Charged Particle Optics*, edited by J. Orloff (CRC Press, Boca Raton, FL, 1997), p. 275.
[13] G. H. Jansen, Adv. Electron. Electron Phys., Suppl. 21 (1990).
[14] J. E. Barth and M. D. Nijkerk, Nucl. Instrum. Methods Phys. Res. A **427**, 86 (1999).
[15] P. Faber and S. Henstra, IMAGE PROGRAM, FEI Company, Hillsboro, USA.
[16] M. S. Bronsgeest, J. E. Barth, L. W. Swanson, and P. Kruit, J. Vac. Sci. Technol. B **26**, 949 (2008).
[17] B. Lencová and G. Wisselink, ELECTROSTATIC LENS DESIGN PROGRAM PACKAGE, v3.70, 2002.
[18] D. R. Kingham and L. W. Swanson, Appl. Phys. A **A34**, 123 (1984).
[19] R. L. Seliger, J. W. Ward, and R. L. Kubena, Appl. Phys. Lett. **34**, 310 (1979).
[20] G. D. Alton and P. M. Read, J. Phys. D **22**, 1029 (1989); Nucl. Instrum. Methods Phys. Res. B **54**, 7 (1991).
[21] G. L. R. Mair, R. G. Forbes, R. G. Latham, and T. Mulvey, *Microcircuit Engineering '83* (Academic, London, 1983), p. 171.